Determining Selected Tropical Cyclone Characteristics Using QuikSCAT's Ultra-High Resolution Images

Faozi Saïd, *Member, IEEE*, and David G. Long, *Fellow, IEEE*

***Abstract*—Operational SeaWinds on QuikSCAT data can be enhanced to yield a 2.5 km ultra-high resolution (UHR) wind product, which can be used to help estimate tropical cyclone (TC) characteristics such as TC center and wind radii. This paper provides the results of two studies in which the QuikSCAT UHR wind product's effectiveness in estimating these TC characteristics is evaluated. First, a comparison is made between an analyst's choice of center location based on UHR images and interpolated best track position. In this analysis, the UHR images are divided into two categories based on the analyst's confidence level of finding the center location. In each category, statistical error quantities between the analyst's choice of center location and interpolated best track location are computed. UHR images within the high-confidence category can provide, for a given year and basin, mean error distance as small as 19 km with a 10 km standard deviation.**

Second, a comparison of QuikSCAT's performance in estimating wind radii is made. QuikSCAT's performance is gauged against the H*wind dataset and the extended best track (EBT) dataset. Results show that QuikSCAT UHR data yields the correct 34 kt wind radius most of the time regardless of the TC category when compared to both H*wind and EBT, whereas the 50 kt and 64 kt wind radii estimates do not always agree with H*wind and EBT. A more sophisticated method is implemented to automatically estimate wind radii based on a model fit to QuikSCAT data. Results from this method are compared with EBT wind radii. The 50 kt and 64 kt wind radii obtained from QuikSCAT model fit are generally highly correlated with EBT estimated wind radii.

***Index Terms*—Atmospheric modeling, radar remote sensing, sea surface, tropical cyclones.**

I. Introduction

HURRICANES, a particular type of tropical cyclone (TC), are one of the most complex weather phenomena tracked by weather forecasters. Their genesis usually takes place over warm oceans within the tropics from weak disturbances. With the right conditions, TCs can gradually increase in size and strength, and potentially become dangerous as they get closer to populated areas. It is therefore crucial to provide to the population adequate warnings, advisories, and precise weather forecasts so as to protect life and property as much as possible.

Manuscript received December 10, 2009; revised March 22, 2011; accepted March 26, 2011. Date of publication May 16, 2011; date of current version December 14, 2011.

The authors are with the Microwave Earth Remote Sensing Laboratory, Brigham Young University, Provo, UT 84602 USA (e-mail: long@ee.byu.edu).

Color versions of one or more of the figures in this paper are available online at http://ieeexplore.ieee.org.

Digital Object Identifier 10.1109/JSTARS.2011.2138119

Hurricane forecasting cannot effectively occur without the use of instruments and sensors to help monitor, measure, analyze, and predict atmospheric processes such as hurricanes. In this paper, we are interested in evaluating the performance of the SeaWinds scatterometer, which is installed on the QuikSCAT satellite platform, for TC wind analysis. The SeaWinds scatterometer (commonly referred as QuikSCAT) is designed to infer wind speed and direction over the ocean from radar backscatter measurements. QuikSCAT wind products were originally destined for research purposes; however, QuikSCAT products have been used by the weather forecasting community throughout the world, starting a few years after becoming operational in 1999 [1]. Prior to QuikSCAT use, weather forecasters used European Remote Sensing (ERS) scatterometer data [2]. Originally designed for a three-year mission, the highly successful QuikSCAT provided continuous wind data for ten years after its launch.

It is desired to provide a comprehensive study of QuikSCAT's effectiveness in determining two specific TC parameters: TC center location and wind radii. These TC parameters help determine the TC size, intensity, and potential zone of destruction. In this paper, analysis of QuikSCAT performance in estimating these parameters is explored. A simple method to automatically estimate wind radii is also presented and evaluated.

The paper is organized as follows. Background information about SeaWinds and its available wind products are discussed in Section II. Section III provides a comprehensive analysis of QuikSCAT UHR images' effectiveness in identifying TC center location. This evaluation is done for all TC cases in the Atlantic basin since QuikSCAT became operational from 1999 through 2008. Finally in Section IV, TC wind radii are manually estimated and visually compared with H*wind and the extended best track (EBT) datasets. A data modeling technique is also introduced to enable wind radii estimation in an automated fashion. Performance is measured against the EBT dataset. Section V discusses the availability of QuikSCAT winds for TC analysis. Section VI concludes this paper by summarizing the various analyses presented.

II. Background

A. *Scatterometer SeaWinds on QuikSCAT*

The QuikSCAT satellite was launched on 19 June 1999 and remained fully operational until 23 November 2009. QuikSCAT is the first wind-vector scatterometer using a dual scanning pencil-beam rotating antenna. QuikSCAT operates at a single

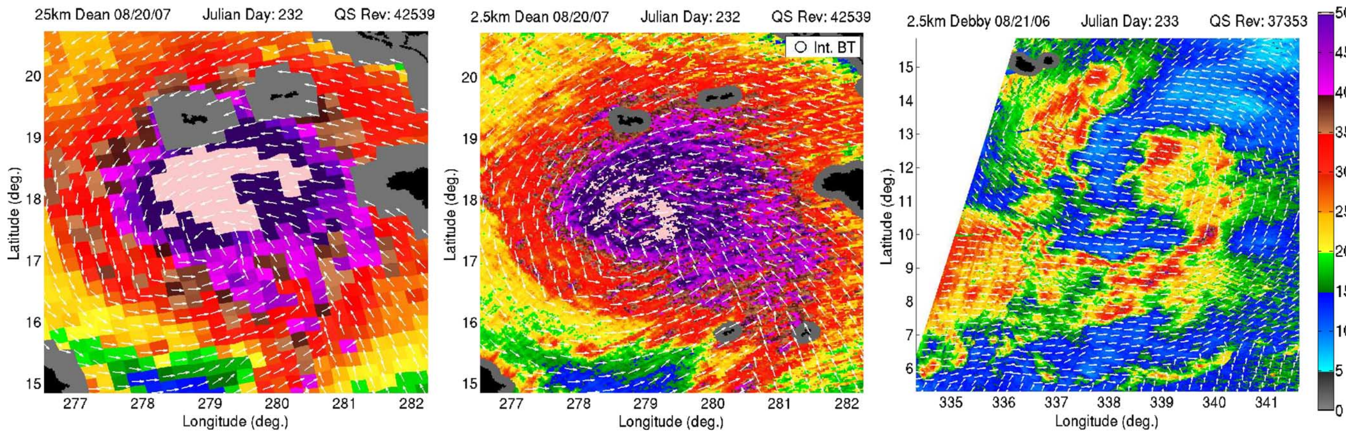

Fig. 1. Wind speed and direction fields plotted (left) on a 25 km grid (L2B) for TC Dean on 20 Aug. 2007, (center) on a 2.5 km grid (UHR), and (right) for TC Debby on 21 Aug. 2006. White arrows represent the L2B wind direction field. Note that UHR images (center and right) contain UHR wind speed field overlaid with L2B wind direction field. Color scale is in m/s.

Ku-band frequency of 13.4 GHz and flies on a sun-synchronous polar orbit 803 km above the earth [3]. This sensor has been designed to measure the normalized radar backscatter (σ°) over the ocean. σ° measurements are collected over a 1800 km wide swath at two nominal incidence angles, 46° (h-pol) and 54.1° (v-pol). This configuration improves wind direction determination, particularly in mid-swath (about 200–700 km on either side of the satellite track) as four types or "flavors" of σ° measurements are possible: inner-forward, outer-forward, inner-aft, and outer-aft. However in the far swath, only two flavors of σ° are available, thus reducing quality in wind retrieval in this area [4]. With a high operating frequency like Ku-band, rain contamination can be problematic, particularly when combined with high or low wind speeds. With low to moderate wind speed ($<$15 m/s), backscatter signals are positively biased. This effect is reversed when rain is combined with hurricane force wind ($>$32 m/s) [5]–[9].

Since QuikSCAT travels at about 7 km/s, each orbit is about 101 minutes long which results in approximately 14 revolutions (revs) per day. With its 1800 km wide swath, QuikSCAT is capable of measuring σ° for about 90% of the ice-free ocean in 24 hours with an exceptionally high rate of successful data collection (more than 98% of the time over its life) [4].

B. QuikSCAT Standard L2B Product and the Ultra-High Resolution Product

When raw telemetry data from QuikSCAT is processed and analyzed, it is made available near-real time to the scientific community for distribution as various geophysical data products. These products are organized in different levels (Level 1 B through Level 2 B). The Level 2 B (L2B) data product provides ocean wind vectors in a 25 km swath grid [10]. A real-time version of the Level 2 B product, known as Merged Geophysical Data Record (MGDR), is produced by the National Environmental Satellite, Data, and Information Service (NESDIS) part of the National Oceanic and Atmospheric Administration (NOAA) [11].

This paper uses the L2B product, which is referred to as the QuikSCAT standard L2B product; however, results are similar when using the MGDR product. The L2B and MGDR products are commonly used by various weather and research centers throughout the world. For example, the Marine Prediction Center (now called the Ocean Prediction Center) forecasters have been using this data extensively since July 2001 to help ensure the safety of ocean-crossing commercial ships and other types of vessels traveling on the high seas [1]. Hurricane forecasters have also been using QuikSCAT data since the 2000–2001 hurricane season to help identify TC characteristics and help in early detection of tropical depressions.

With the standard L2B product, images of hurricanes can be obtained by plotting the wind speed and direction fields (see Fig. 1). Though a few TC structural features are identifiable in this figure (such as the eye center, eyewalls and TC size), ambiguity selection errors and low resolution can hinder the ability to distinguish such features. To improve the spatial resolution, a resolution enhancement algorithm can be used to generate high resolution backscatter images which can ease TC feature identifications [12]–[16]. The UHR algorithm takes advantage of the spatial overlap of σ° measurements to enhance the spatial resolution of the σ° values used to estimate the wind. The final product obtained from this technique is called the ultra-high resolution (UHR) wind product and is reported on a 2.5 km swath grid [16], [17] . This product is made available through the National Environmental Satellite, Data, and Information Service (NESDIS) "manati" web site (http://manati.orbit.nesdis.noaa.gov/quikscat/) and from the Scatterometer Climate Record Pathfinder web site (http://www.scp.byu.edu/data/Quikscat/HRStorms.html). Although prone to noise and rain contamination, the general patterns and TC centers are much more readily apparent in the UHR wind fields than conventional resolution winds, as revealed in Fig. 1.

C. Best Track Data

So-called "best track" information is used as ground truth for TC center and category identification. Best track data is provided by the National Hurricane Center (NHC) and the Joint Typhoon Warning Center (JTWC) for the five major ocean basins (Atlantic, Indian, Southern Hemisphere, Western, and Eastern Pacific). For each named TC, the best track dataset provides the center location, maximum sustained wind speed, and atmospheric pressure at the center every six hours over the TC lifetime. A limitation of this dataset is that it does not contain information about storm structure. The 'extended' best track data (EBT) is a supplement to best track data. The additional parameters EBT contains are maximum radial extent of 34, 50, and 64 kt wind in four quadrants; the radius of maximum wind; the eye diameter if available; and pressure and radius of the outer closed isobar [18]. These datasets are usually available several months after a given hurricane season, since several different types of post-analysis are required to confirm and set the best possible TC track dataset. Though the best track and EBT datasets are used in this study as ground truth, there are two key factors to keep in mind: first, QuikSCAT MGDR winds may have been included at times in the best track data development, which may limit its utility as an independent analysis tool; second, best track data are not immune from errors. Despite such limitations, best track data and EBT are useful tools to validate QuikSCAT UHR TC center locations and wind radii estimation.

III. TC Center Identification

Both standard 25 km and UHR wind products are operationally retrieved from SeaWinds on QuikSCAT for each named TC. Best track data are used to co-locate QuikSCAT passes with TC center locations. Since best track data provide center locations only every six hours for a given TC, a parametric spline interpolation technique is used to approximate the best track center location corresponding to the time of each QuikSCAT pass over a TC. No restriction was set on location or basin in this study. All available reported best track data are used to obtain as many collocations as possible in a given basin. The TC category is identified from the best track data.

Two sets of images are created at different resolutions for each given QuikSCAT pass of a TC within a basin. The first set (L2B) contains wind field images with a standard resolution of 25 km, whereas the second set (UHR) contains winds retrieved at an ultra-high resolution of 2.5 km. Rain is not flagged. Using a simplistic subjective approach, each image was manually analyzed by a student to locate the center of the TC [19]. Note that the analyst did have significant prior experience in this task and that the manual center location was done without prior knowledge of the best track locations. The analyst's TC center identification is exclusively based on QuikSCAT wind products, and primarily based on the general flow pattern contained in the wind speed field, with a mild consideration of the general wind direction field; alternate wind solutions (ambiguities) are not used in this paper. The center is subjectively based in a concentration of higher wind speeds, at central local minimum if present, see below. Center positions are separately estimated from both L2B and UHR wind speed images.

While we recognize that more sophisticated center algorithms [20] and other sensor data could be used, we have adopted a very simple QuikSCAT-only approach to evaluate the effectiveness of just the QuikSCAT data. Using the estimated center locations, we compare the error distance between the manual analyst center locations to best track's in order to evaluate QuikSCAT's effectiveness in TC analysis in the following.

A. Confidence Level With UHR Images

Since it is subjectively easier to identify the TC center location at higher resolution, UHR image analysis is divided into two categories depending on the confidence level of identifying the center in each image. The first category includes images in which we have high confidence in the TC center location; the second category includes images where TC center identification is possible but with a low to medium level of confidence. In general, the latter category includes images of underdeveloped TCs, TCs with equivocal wind patterns, TCs halfway over land, or images which only partially cover a TC. The low confidence category also includes TCs with a concentrated area of maximum winds but no apparent central wind minimum.

The right panel of Fig. 1 is a good example of an underdeveloped TC. This UHR image is considered low confidence because no well-defined center can be identified; it is difficult to decide where the center of the TC is. On the other hand, the center panel of Fig. 1 is a good representation of a high-confidence case. In this figure, the center is unambiguously identifiable. We note that these confidence levels are defined subjectively with the analyst deciding whether the center location is of low or high confidence.

For each confidence category, a table with the standard deviation, mean, and median of the error distance (in kilometers) between the manual analyst center location and the interpolated best track center location is created. Histograms based on these error distances are plotted and analyzed for the full QuikSCAT mission. The following subsection describes results obtained for the year 2006 in the Atlantic (ATL) basin.

B. Results for the Year 2006 in the ATL Basin

In 2006, ten named TCs swept through the Atlantic basin. For these ten TCs, 112 UHR and 98 L2B images from SeaWinds on QuikSCAT were analyzed (not as many L2B images were retained as it was impossible at times to identify a TC center in an L2B image). An error distance histogram is plotted for each set of images [see Fig. 2(a) and 2(b)]. The error distance represented in these plots is between the interpolated best track center location and the analyst's location based on the QuikSCAT images. Comparing both histograms, we notice a 12 km improvement in the mean error using all UHR images over standard resolution images as well as a slight improvement in the median and standard deviation. Yet, close analysis of Fig. 2(b) indicates that the error between the analyst and the interpolated best track center location is still significant for a high number of UHR images (mean error of 54 km). The statistics are further analyzed and split into the two confidence categories described in Section III-A.

1) Low-Confidence Category: The analyst concluded that 77 out of the 112 UHR images for the Atlantic basin fall in the low-confidence category. A histogram of error distances for these low-confidence images is shown in Fig. 2(c). For this category, the mean error distance is 67 km (20% higher than the mean error for all UHR images combined), with a median of 55 km and a standard deviation of 44 km. Despite the low-confidence criteria given to these images, nearly half of the images have an error distance below 50 km (37 out of 77). Thus, even if the analyst is not sure where the center location of a TC is,

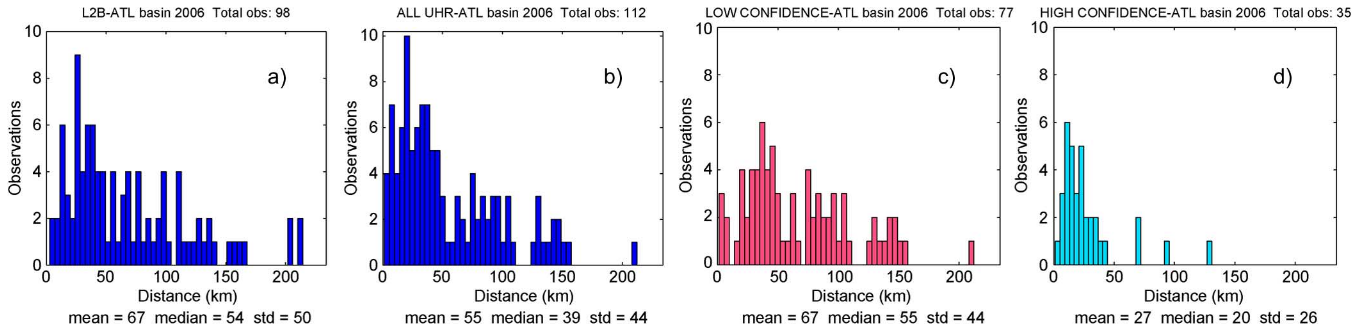

Fig. 2. Error distance between interpolated best track and analyst's center location for all TCs in the Atlantic (ATL) basin in 2006 (see plots (a) and (b)—all L2B and all UHR, respectively). Plots (c) and (d) represent the error distance between interpolated best track and analyst's center location for the low and high-confidence UHR images, respectively.

TABLE I
STATISTICAL RESULTS FOR L2B AND UHR IMAGES FOR THE ATL BASIN IN 2006

	Mean error (km)	Median (km)	Stand. dev. (km)
All L2B	67	54	50
All UHR	55	39	44
Low confidence	67	55	44
High confidence	27	20	26

reasonable results can be obtained for the center location. Since low-confidence cases are common for low intensity TCs and during cyclogenesis, these results show that an analyst can accurately locate the TC center from QuikSCAT alone at least 50% of the time.

2) High-Confidence Category: A total of 35 observations in the Atlantic basin were considered of high confidence. In this case, the mean error distance to the interpolated best track center location is 27 km; the median and standard deviation are respectively 20 km and 26 km [see Fig. 2(d)]. Table I regroups these statistics. The mean error distance obtained from the high-confidence set of observations shows a noticeable improvement from both the low-confidence and the overall set of UHR observations. From 55 km (all UHR images combined), the mean error decreases to 27 km which is a 51% improvement. Typically, hurricane eyewalls of developed TCs have a diameter of 20 to 60 km [21]. Thus a 27 km mean error for the high-confidence set of observations means that on average the analyst can easily pinpoint the center of a TC. Even by taking into account the 26 km standard deviation, the analyst can find the center of a TC almost in every single high-confidence UHR image. Even with such good results, it is interesting to note that four observations have an error distance greater than 60 km [see Fig. 2(d)]; these errors range from 68 km to 131 km. Such large errors are surprising. Further extensive analysis of these observations led us to the conclusion that problems in the best track data are the most likely the prime source of error since the EBT reported locations were outside of the high wind speed region. By neglecting these four unusual error distances greater than 60 km, the mean error distance for the high-confidence category decreases from 27 km to approximately 19 km (a 65% improvement compared to all UHR images combined); the median decreases from 20 km to 18 km and the standard deviation from 26 km to 10 km. For this particular basin, high-confidence UHR images represent 31% of all UHR images analyzed.

TABLE II
STATISTICAL RESULTS FOR LOW-/HIGH-CONFIDENCE UHR IMAGES IN THE ATL BASIN FOR THE PERIOD 1999–2008 (DISTANCE IN km; LC AND HC REFER TO LOW CONFIDENCE AND HIGH CONFIDENCE, RESPECTIVELY)

ATL basin	99	00	01	02	03	04	05	06	07	08
LC Mean	70	61	60	57	52	70	50	67	49	44
LC Med.	44	52	38	42	40	54	53	55	45	34
LC Stdv.	69	53	64	54	53	70	36	44	36	32
Total obs.	38	31	43	27	84	31	44	77	48	75
HC Mean	18	24	25	24	21	19	23	19	24	22
HC Med.	13	21	23	19	16	15	21	18	18	20
HC Stdv.	15	19	15	17	14	16	15	10	17	14
Total obs.	42	60	55	42	154	76	115	31	25	45

C. Results for the Years 1999 to 2008 in the ATL Basin

For the ATL basin, the low- and high-confidence categories encompass, respectively, 499 and 646 UHR images over the period of 1999–2008. Table II shows the statistical results (mean error distance, standard deviation, median as well as the number of low/high-confidence observations) for the years 1999 through 2008. The high-confidence error plot shows a fairly small and consistent average in the error distance of the TC's center position which in turns reinforces the reliability of QuikSCAT data. For the low-confidence set of images, the mean is between 44 km and 70 km, while the high-confidence mean is between 15 km and 25 km. As before, few observations have very large error distances. A total of eight different cases (spread out in the years 2000, 2001, and 2004) have such error distances. After extensive analysis, it was determined that best track data reports for these particular cases were likely erroneous. These cases have been excluded from Fig. 3. The corresponding error plots of the yearly means with their respective standard deviation can be found in Fig. 3.

We conclude that an analyst accurately finds the TC center location in all high confidence QuikSCAT UHR images. Between 1999 and 2008, 56% of all UHR images for the ATL basin were considered of high confidence.

IV. WIND RADII ESTIMATION

A wind radius is defined as the largest radius at a fixed wind speed in a quadrant around a TC center. The wind speeds at which wind radii are estimated are 34, 50, and 64 kt. Wind radii are valuable metrics used by NHC to help estimate the size, storm surge, TC intensity, and possible impact of a given TC. When TCs are reachable by aircraft, wind radii estimates are

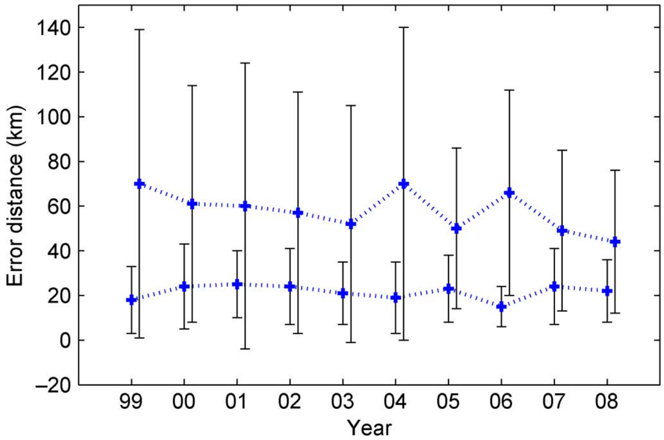

Fig. 3. Yearly mean error plots for the UHR images in the Atlantic basin from 1999 to 2008. The curve with large standard deviations and yearly means greater than 60 km corresponds to the low-confidence category; the other with lower yearly means and standard deviations corresponds to the high-confidence category.

generally derived from instruments placed on aircraft which fly through TCs in an alpha pattern as far as 105 nautical miles from the center [22]. With the use of GPS dropwindsonde and on-board radiometers/scatterometers, these aircraft are capable of measuring atmospheric pressure, temperature, humidity, and wind speed and direction along their path. These measurements can be sent to the TC forecasters at the NHC for immediate analysis.

Because aircraft cannot fly over the whole TC, resolution of the aircraft-inferred wind speed field can be low in a given TC quadrant. Furthermore, when TCs are out of reach from these aircraft, forecasters rely heavily on the relatively few buoys scattered over the Atlantic ocean and scatterometers to estimate wind radii. The latter can supply substantially more data for a given TC compared to buoys. NHC estimates of wind radius are subjective and therefore it is of interest to develop and use automated algorithms to estimate wind radii using QuikSCAT UHR wind product and analyze their performance. Prior to performing such a task, a comparison of wind radii obtained from QuikSCAT is made with co-located H*Wind and the extended best track (EBT) dataset.

*A. Comparison With H*Wind and EBT Data*

The hurricane research division (part of NOAA) has been working since 1996 on a project called H*wind [23]. The purpose of this project is to develop an integrated tropical cyclone analysis system using data gathered from various platforms (including QuikSCAT). The experimental product includes wind data (surface speed and direction fields) which are mostly used for research purposes. H*wind products are considered to be reasonably accurate with a 10 to 20% error; this error margin is attainable only when aircraft data are used in the generation of H*wind data, which is only possible when TCs are reachable from land-based aircraft. This limits the number of possible spatial and temporal co-locations between QuikSCAT passes and H*wind between 1999 and 2008 to only 47 TC cases (co-locations were done by [24]) in the ATL basin where H*wind is mainly available. Table III summarizes the number of co-locations per intensity category (the latter being provided by best track data). It is important to note that QuikSCAT data was excluded in the generation of the 47 co-located H*wind data so as to provide a fair comparison between the two products.

TABLE III
NUMBER OF QUIKSCAT TC CASES AND CO-LOCATIONS PER INTENSITY CATEGORY WITH H*WIND AND EBT (1999–2008)

Int. cat.	Quik. TC cases	H*wind Co-Loc.	EBT Co-Loc.
Trop. Dep.	180	0	0
Trop. Storm	559	10	20
Hurr Cat 1	214	9	11
Hurr Cat 2	71	6	2
Hurr Cat 3	58	5	3
Hurr Cat 4	61	12	11
Hurr Cat 5	—	5	2
Extratropical	209	0	2
Total	1352	47	51

QuikSCAT wind radii are determined visually for each co-location and compared with H*wind. To simplify the analysis, the comparison is conducted only for the North East (NE) quadrant of each co-located TC. QuikSCAT wind radii determination is done using a scatterplot of QuikSCAT wind speed versus distance from the center for a given quadrant (see Fig. 4). Since wind radii are determined by finding the maximum possible wind speeds at a given radius, QuikSCAT wind speed on this plot is based on its four largest values for each distance. These wind speed maxima, however, should be interpreted with caution since UHR wind product is inherently noisy and may be rain-contaminated [16]. We note that rain flagging is not used in this paper. Note Fig. 4 also shows H*wind wind speed field (left-most plot) as well as the scatterplot of H*wind wind speed versus distance from the center, overlaid with QuikSCAT wind speed maxima, (right-most plot) for TC Ivan on 14 Sep. 2004. The middle plot of Fig. 4 represents the corresponding QuikSCAT UHR wind speed field.

For each TC co-location between H*wind and QuikSCAT, similar scatterplots are created and used to determine QuikSCAT wind radii. Results of this analysis are represented on the top three plots of Fig. 5. Each plot shows correlation between H*wind and QuikSCAT wind radii at a given wind speed (i.e., 34, 50, and 64 kt). The first two plots show a consistent agreement between the two datasets. However, it is clear that poor results are obtained for the 64 kt wind radii; in this latter case, QuikSCAT tends to underestimate high winds, which should be expected due to scatterometer GMF limitations, particularly in the presence of rain [5], [6].

This preliminary wind radii analysis between H*wind and QuikSCAT yields the following points:

- QuikSCAT wind speed is often erroneous in high rain rate areas. It is therefore very useful to identify and exclude such areas prior to visually determine a wind radius.
- Isolated thunderstorms of variable size can be present in the proximity of a TC core, which may lead to wind speed overestimation and larger than necessary 34 kt wind radii. If the effects of these mesoscale weather systems are ignored, 34 kt wind radii estimated from QuikSCAT are usually very similar to H*wind 34 kt wind radii.
- QuikSCAT shows a much more complex wind field than suggested by H*wind, though the overall wind speed

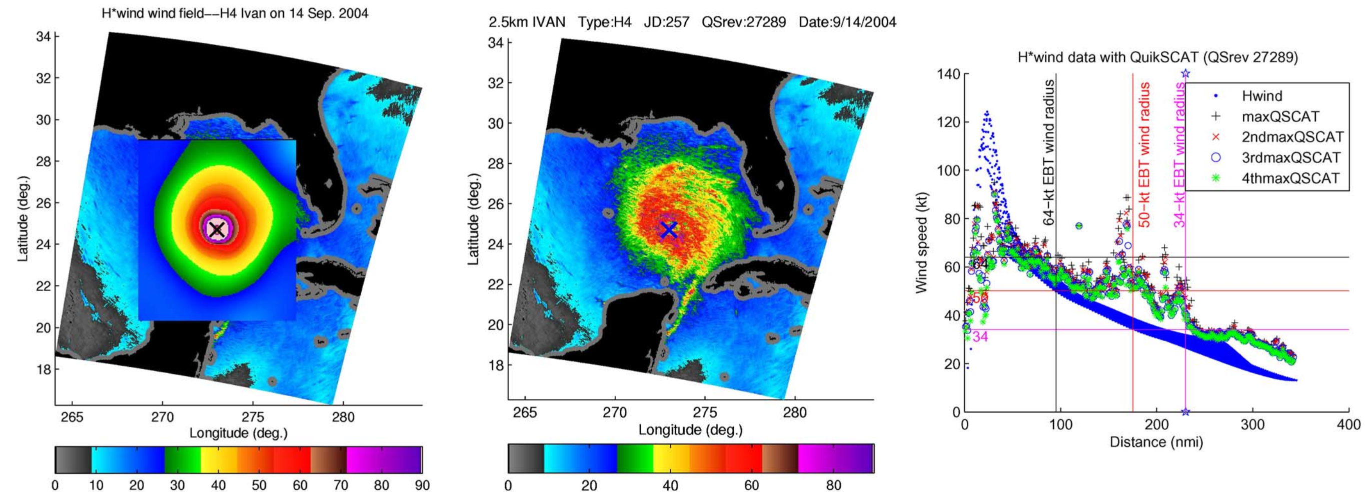

Fig. 4. Plots of H*wind and QuikSCAT UHR wind speed fields for TC Ivan on 14 Sep. 2004 (far left and center plots, respectively). Color scale is in knots. The far right plot is a scatterplot of H*wind wind speed versus distance from the center overlaid with QuikSCAT wind speed maxima for the North East quadrant of the TC only. Note the three EBT wind radii shown by the vertical lines. In this plot, the 34 kt QuikSCAT wind radius is found to be close to 300 nmi; while EBT is around 225 nmi and H*wind around 210 nmi.

versus radius shape is maintained. There is more potential information available due to the higher resolution QuikSCAT wind product.

- As with TC Ivan (see Fig. 4), it is possible to obtain high correlation between the two datasets in extreme cases (hurricane-type TC) especially for the 34 kt and 50 kt wind radii.
- QuikSCAT wind speeds are severely underestimated for most of the TC core in extreme wind conditions (i.e., H1–H5).

A similar analysis is carried out with the EBT dataset, which is a supplement to best track [25]. This dataset contains, in addition to what best track data already provides, the radius of maximum wind speed, center diameter, pressure of the outer closed isobar (hPa), radius of the outer closed isobar (nmi), and radii of 34, 50, 64 kt for each quadrant of the TCs. Since EBT provides these metrics every six hours during any TC lifetime, 169 co-locations for the ATL basin (1999–2008) between the EBT dataset and QuikSCAT UHR are possible. Using only the EBT dataset west of 55 longitude (which is more reliable thanks to available aircraft data), and because of land contamination and underdeveloped TC conditions, the number of useful co-locations is 51 (see Table III).

For illustration purposes, EBT wind radii are represented with vertical lines in Fig. 4. For all QuikSCAT-EBT co-locations, QuikSCAT wind radii are determined the same way as described in the previous analysis with H*wind. Results can be found on the three lower scatterplots of Fig. 5. The following points summarize the observations made during QuikSCAT-EBT wind radii analysis:

- A recurrent problem is underestimated QuikSCAT wind speed around the eye wall. This may explain the absence of 50 kt and/or 64 kt wind radii from QuikSCAT, especially in extreme cases.
- The 34 kt wind radii, however, are highly correlated with EBT wind radii but occasionally are overestimated (see Fig. 5).
- It is hard to interpret why at times QuikSCAT has no difficulty estimating the radii of wind speeds close to or above 50 kt, while most of the time the estimates are inaccurate.
- Hurricane Dean (cat 1) case provides some interesting results: the 34 kt and 64 kt wind radii from QuikSCAT correlate reasonably well with EBT wind radii; however the 50 kt is underestimated by approximately 40 nmi. There is no clear justification as to why such results are obtained. However, it is interesting to note that wind radii reported by hurricane analysts (i.e., EBT wind radii) are subjective estimates and may not indicate direct wind radius measurements from any instrument; a subjective margin of error may have been added to the actual wind speed measurements received.
- In some rare cases (for example, Hurricane Katrina cat 5 on 28 August 2005 at 1127 UTC), the three wind radii estimated by QuikSCAT are very close to the EBT wind radii, even in extreme wind speeds. As mentioned earlier, heavy rain rates may have positively biased QuikSCAT wind speed, though this cannot be confirmed.

While limitations have been identified when using QuikSCAT UHR wind product to estimate wind radii, this preliminary analysis shows that there is a strong potential for using QuikSCAT UHR winds to help determine wind radii. It is important to note that these analyses have been based solely on the use of the QuikSCAT wind speed maxima for each of the four radii from the center. These values are noisy and should be used with care. Yet, this data yields a correct 34 kt wind radius most of the time regardless of intensity category when compared to both H*wind and EBT. The 50 kt and 64 kt wind radii estimated from QuikSCAT UHR data do not always match H*wind nor EBT and rain bands can adversely affect QuikSCAT wind speed estimation. Despite these limitations, we can use data modeling techniques to estimate QuikSCAT wind radii in an automated fashion as described below.

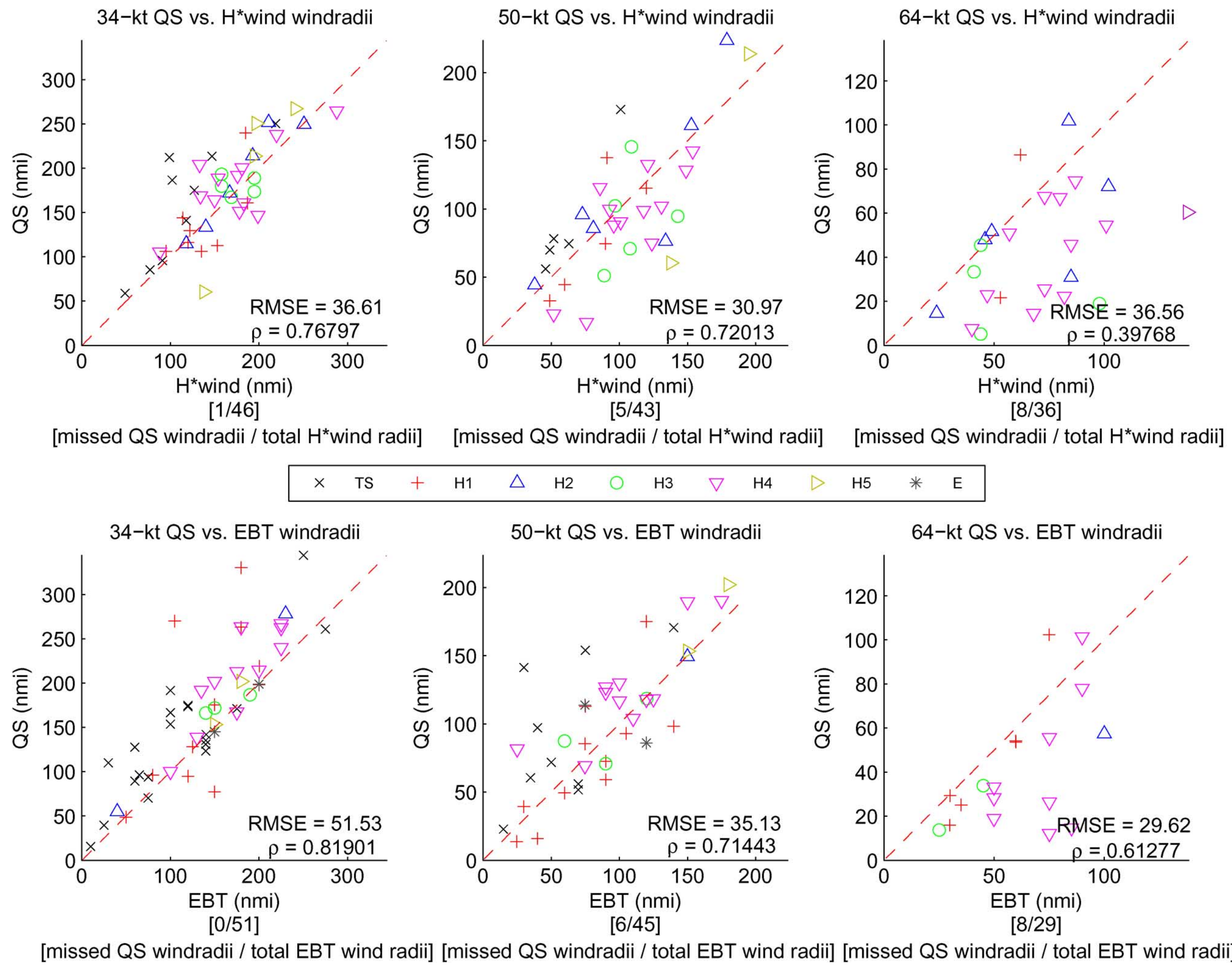

Fig. 5. Scatterplots of NE quadrant 34, 50, 64 kt QuikSCAT wind radii vs. H*wind (see top row), and QuikSCAT wind radii vs. EBT (see bottom row). The top row and bottom row plots are based on all TC co-locations between QuikSCAT and H*wind, and between QuikSCAT and EBT from 1999 to 2008, respectively. Note that a 'missed' wind radii corresponds to an instance where QuikSCAT wind speed profile never reaches one of the 34, 50, or 64 kt wind speeds.

B. Wind Radii Estimation Using a Data Modeling Technique

A simple method is now implemented to estimate wind radii based on a model fit to QuikSCAT data. The purpose of using such a method is to help automate the wind radii estimation process. While we are aware that there are sophisticated methods of estimating such a metric [16], [26], our goal is to provide a simple objective method for estimating QuikSCAT wind radii in each quadrant for comparison to the EBT wind radii.

1) Wind Radii Estimation Procedure: The proposed wind radii estimation procedure is fairly simple to implement. Two major elements constitute the backbone of this estimation process: the use of a static model and a transfer function. First, a model based on empirical data from all QuikSCAT TC passes from 1999 to 2007 is used to estimate the mean wind speed versus radius from the TC center for a given intensity category. Since wind speed inferred from QuikSCAT data is a mean wind speed [27], it is necessary to convert the model wind speed to an equivalent maximum sustained wind speed. This enables the wind radii estimation from a model fit to QuikSCAT data to be validated against the EBT data set. This is accomplished with a simpled transfer function based on H*wind co-located TC cases with QuikSCAT to adjust the model mean wind speed to a maximum sustained wind speed.

2) Model Description: As shown in Section IV-A and [6], at extreme winds the wind speed inferred from the QuikSCAT UHR wind product can be under- or overestimated at times due to heavy rain. This minimizes the effect of noisy measurements. The model uses all QuikSCAT TC passes from 1999 to 2007. The mean wind speed for each distance from the center is found by empirically computing the conditional expectation $E(S|D = d,\ Q = q,\ T = t)$, where S is the wind speed in knots, D is the distance from the center in nautical miles (nmi), Q is a quadrant, and T is a intensity category. Since the conditional expectation $E(S|D = d,\ Q = q,\ T = t)$ and all other density functions used to derive this quantity are always conditioned on Q and T throughout this section, these two variables are implied to simplify notation; i.e., $f_{S,D|Q,T}(s,d|q,t) \equiv f_{S,D}(s,d)$. The model wind speed at each radius from the center is found using the empirical conditional expectation

$$E(S|D = d) = \sum_s s \cdot f_{S|D}(s|d) \qquad (1)$$

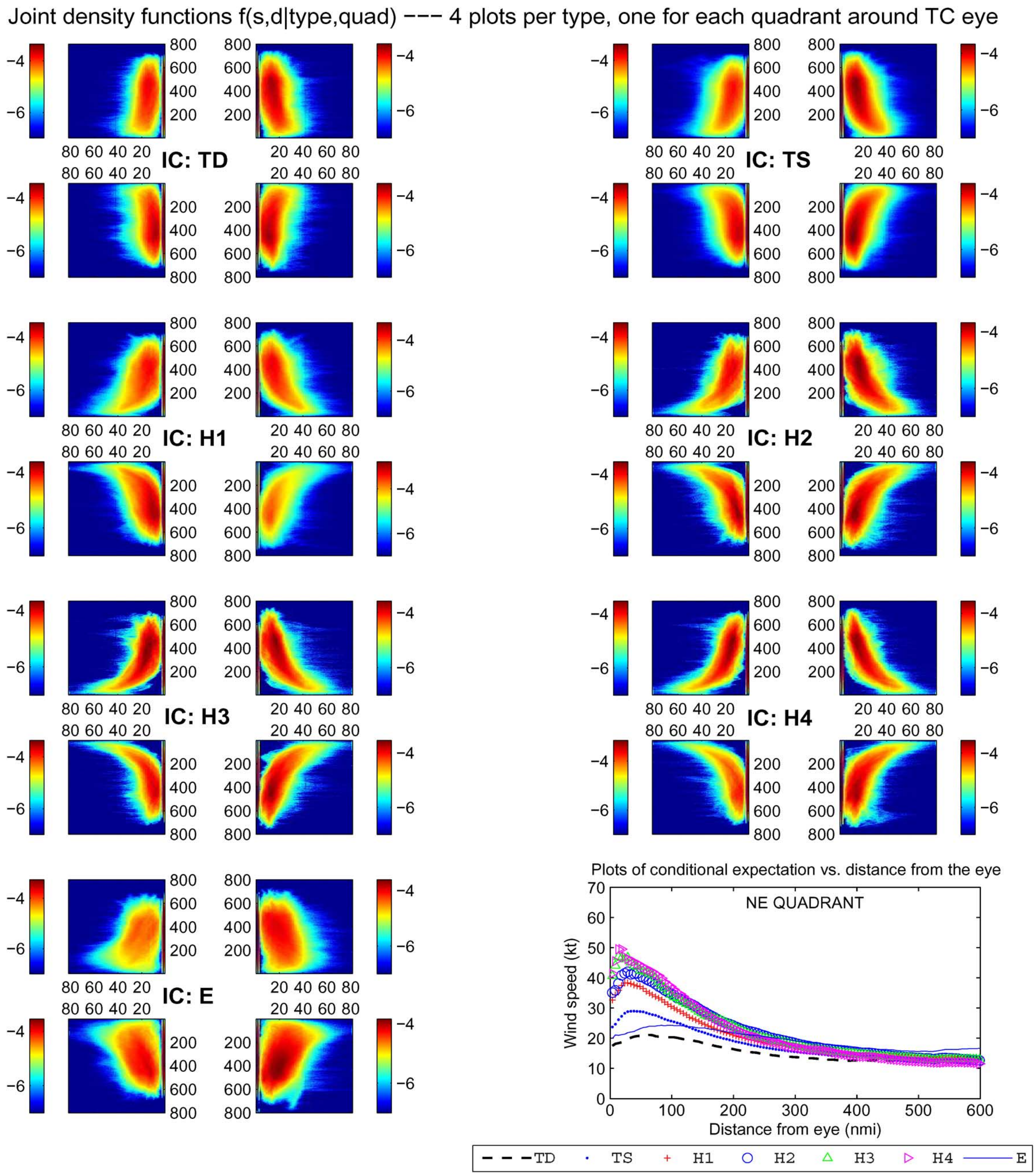

Fig. 6. Histogram-derived joint density functions of wind speed and distance from the center. For each intensity category (IC), four density plots are shown—one for each quadrant. Color scale is in dB. The bottom right plot represents the mean wind speed for each distance from the center for the NE quadrant of all TCs. Seven curves can be found in this plot—one for each intensity category (TD, TS, H1, H2, H3, H4, E).

where $f_{S|D}(s|d)$ is the conditional density function of the wind speed s given the distance d from the center. To compute $f_{S|D}(s|d)$, it is first necessary to determine the joint density function $f_{S,D}(s,d)$. Fig. 6 illustrates the empirical joint density functions of wind speed and distance from the center for each quadrant and intensity category. Note that for a given intensity category, the shapes of the joint density functions are very similar from quadrant to quadrant. However, from one intensity category to another, there is a definite change in curve shapes. This change can be due to significant wind speed changes around the eye's vicinity, and TC size variation between intensity categories.

Using Bayes' rule, it is possible to find the conditional density function of the wind speed given distance from the center, $f_{S|D}(s|d)$

$$f_{S|D}(s|d) = \frac{f_{S,D}(s,d)}{f_D(d)} \tag{2}$$

where $f_D(d)$ is the marginal density function of distance d from the center. This quantity is found using the following identity:

$$f_D(d) = \sum_s f_{S,D}(s,d). \tag{3}$$

Table III shows the number of cases used per intensity category to compute the various density functions necessary to ultimately determine the desired conditional expectations. In the lower right corner of Fig. 6, a plot of the mean wind speed for each distance from the center for the NE quadrant of all TCs is represented. In this plot, seven curves are shown—one per intensity category. Note that the smoothest curves correspond to intensity categories with the most TC cases retrieved, as shown in Table III. We note the relatively low maxima of the mean wind speed curves. This is the result of the Geophysical Model Function, which relates the near-surface wind speed to the QuikSCAT backscatter measurements, clipping at 50 ms^{-1} ($\approx$ 97 kts) [10]. Rain attenuation of high winds may also be a contributor [5], [16].

3) Model Implementation: Since the model described previously is based on the mean wind speed at a given radius, a linear relationship is assumed between the model fit and the wind speed data, i.e.,

$$s_i(d_i) = \alpha + \beta s_m(d_i) \tag{4}$$

where $s_i(d_i)$ and $s_m(d_i)$ represent the data wind speed and the model wind speed, respectively, from the distance d_i to the center. α and β represent the model parameters which control the shape and vertical shift of the model fit curve. These parameters can be found using the minimum mean square error estimation technique (MMSE). Once α and β are determined, obtaining a model fit to the data is possible using the estimated mean wind speed.

Rewriting (4) in matrix form is helpful to estimate the wind speed:

$$\begin{pmatrix} s_1(d_1) \\ \cdots \\ s_i(d_i) \end{pmatrix} = \begin{pmatrix} 1 & s_m(d_1) \\ \cdots & \cdots \\ 1 & s_m(d_i) \end{pmatrix} \begin{pmatrix} \alpha \\ \beta \end{pmatrix} \equiv \underline{S} = \underline{D}\underline{A}. \tag{5}$$

The model parameters α and β (in $\underline{A}$) can be found using the pseudo-inverse technique:

$$\underline{A} = (\underline{D}^T \underline{D})^{-1} \underline{D}^T \underline{S}. \tag{6}$$

This equation provides a minimum mean square error solution to the system of linear equations as shown in (5), and a model fit to the data is obtained when $\underline{A}$ is found.

*4) Bias Adjustment Using H*wind Data:* The estimation of a wind radius for a given wind speed requires knowledge of the maximum sustained wind speed at each radius from the center. Therefore, it is necessary to adjust QuikSCAT wind speed to be consistent with a 1-minute maximum sustained wind speed prior to estimating wind radii from it. Since our model fit is based on mean wind speeds, the standard deviation of the mean wind speed model is added at each radius. We note that best track wind radii are estimated based on 1-minute maximum sustained wind speeds, while the reported QuikSCAT wind speed is roughly equivalent to a 8–10 minute mean surface wind [27].

H*wind data provide a 1-minute maximum sustained wind speed field for each available TC co-location with QuikSCAT data. To ensure data compatibility between QuikSCAT and H*wind and best track, we use all H*wind and QuikSCAT TC co-locations to perform a simplistic bias adjustment of the model fit wind speed based on H*wind wind speed. The top scatterplot of Fig. 7 shows H*wind versus the estimated wind speed (from the updated model fit) for the 47 co-locations found (see Table III). It can be seen that for distances close to the center (10–60 nmi), the model fit based on mean wind speed plus standard deviation generally underestimates wind speed. As distance from the center increases, the model fit overestimates wind speed. Note the second-order fit to the data in this scatterplot; the coefficients of the second-order fit are used to adjust the QuikSCAT model fit wind speed. The bottom scatterplot of Fig. 7 shows H*wind wind speed versus the

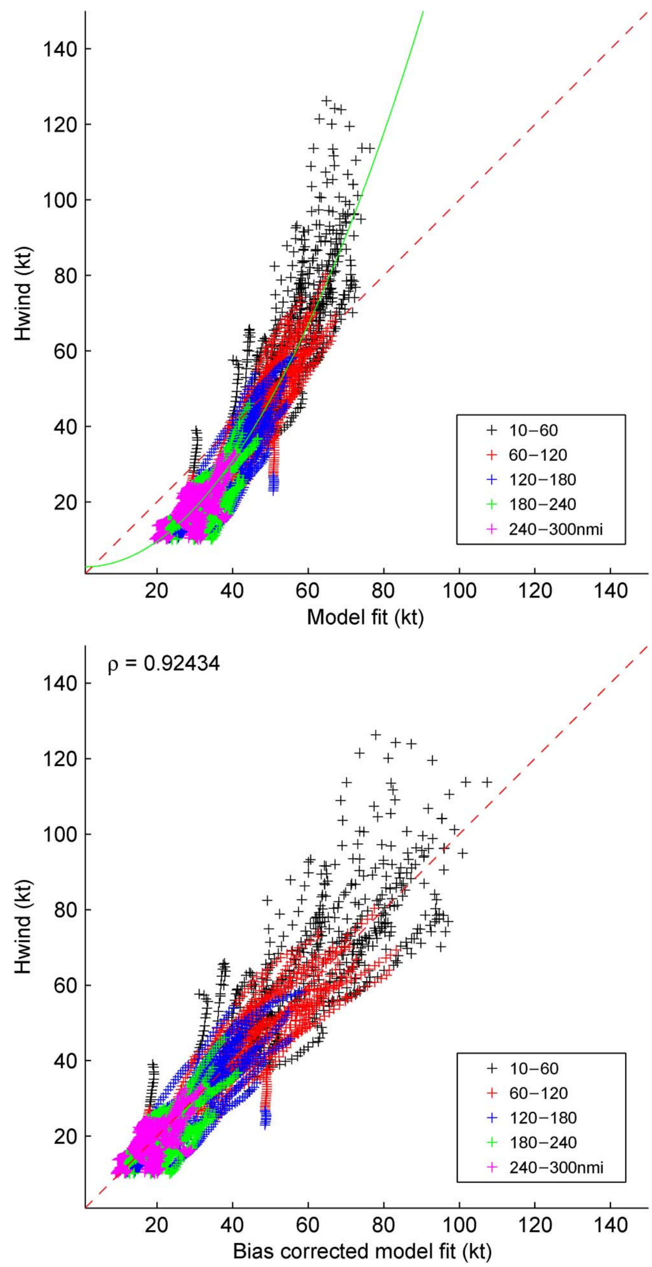

Fig. 7. H*wind versus QuikSCAT wind speed scatterplots at various distance ranges from the center. Note the second-order fit on the top plot. Wind speed is in knots.

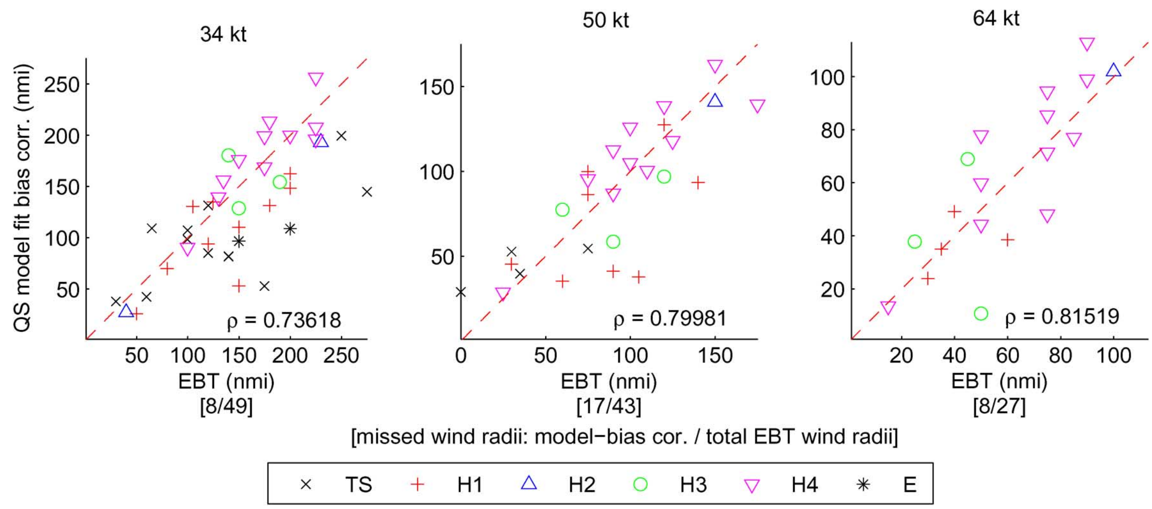

Fig. 8. Scatterplots of 34, 50, and 64 kt wind radii from QuikSCAT adjusted model fit versus EBT. At the bottom of each scatterplot, the number of missed QuikSCAT model fit wind radii is specified. In the lower right corner of each plot, a correlation coefficient ρ is also provided.

adjusted QuikSCAT model fit wind speed. A higher correlation is found between the two sets of data for all distances from the center. Yet, for distances closer to the center, correlation is lower for extremely high wind speeds, which is to be expected due to GMF clipping at 50 m/s [10].

C. QuikSCAT Wind Radii Validation

To evaluate the performance of the wind radii estimation procedure described in this section, we use 49 out of the 51 temporal and spatial co-locations between QuikSCAT and the extended best track (two co-locations refer to type H5 TCs—the model for wind radii for this TC category is not estimated due to the small number of cases).

Fig. 8 shows the scatterplot of 34, 50, and 64 kt wind radii from both QuikSCAT adjusted model fit and EBT. Results obtained from the QuikSCAT adjusted model fit are generally highly correlated with EBT estimated wind radii. It is interesting to note that there are fewer missed 64 kt wind radii than 50 kt (6 versus 15; see Fig. 8). Despite the number of missed wind radii, we can conclude that it may be possible to estimate the wind radius in an automated fashion using the procedure outlined in this section. Once QuikSCAT wind radii are found, they can be analyzed and adjusted by hurricane forecasters based on their extensive experience.

V. QuikSCAT TC Tracking Utility

In the areas where most TCs occur, at most two observations per day are available (in some rare locations such as the Gulf of Mexico, up to three times). Thus, when tracking a TC it may be possible to obtain two UHR images from QuikSCAT daily. However, center locations may not always be identifiable in every image; at times TCs may be only partially covered, partway over land, or incipient. As previously noted, such images may not be useful for TC analysis since the TC centers cannot be determined in these situations.

Our purpose in this section is to evaluate how often QuikSCAT UHR images have been useful for TC center observation over its mission. The analysis is done on a TC-by-TC basis. For each TC, UHR images are classified into two main categories based on the number of QuikSCAT images received per day. Once classified, the usefulness criteria come into play: the images are either considered useful or not based visibility of the TC center. Fig. 9 illustrates the results of this analysis for the Atlantic basin using bar graphs.

Due to the complex nature of this figure, an example is provided below to demonstrate how to interpret it. We desire to analyze in the Atlantic basin TC Olga in 2001 (TC number 15; see third bar graph in Fig. 9). As indicated on the plot, the TC life is 12 days. For 10 out of these 12 days, two co-located images per day are obtained for TC analysis (as shown in the top portion of that plot). Out of these 10 days, 50% of the time both images are considered useful to the analyst; 40% of the time, only one is considered useful, and 10% of the time neither of them are. The bottom portion of the plot shows cases where only one co-located QuikSCAT image is obtained in a day. For TC 15, this occurred twice. Only once in these two days is the obtained image found to be useful for TC analysis. Overall, at least one useful QuikSCAT UHR image per day is available 83% of Olga's TC life, while two useful UHR images per day are available 42% of it. The same analysis can be done on a TC-by-TC basis and is reported in these bar graphs in Fig. 9. It is then possible to appreciate how often, out of the lifetime of a given TC, useful co-located QuikSCAT images of the TC center are obtained.

For more general results, pie charts are provided for each basin (see Fig. 10), which combine all the results obtained from 1999 to 2007. They show the distribution of useful UHR images received daily. The ideal situation is to obtain two useful QuikSCAT observations per day all the time; however, this occurred only 25.7% of the time in the ATL basin (see Fig. 10). Nevertheless, at least one useful UHR image is obtained daily 60.5% (ATL) of the time. Having at least two scatterometers on

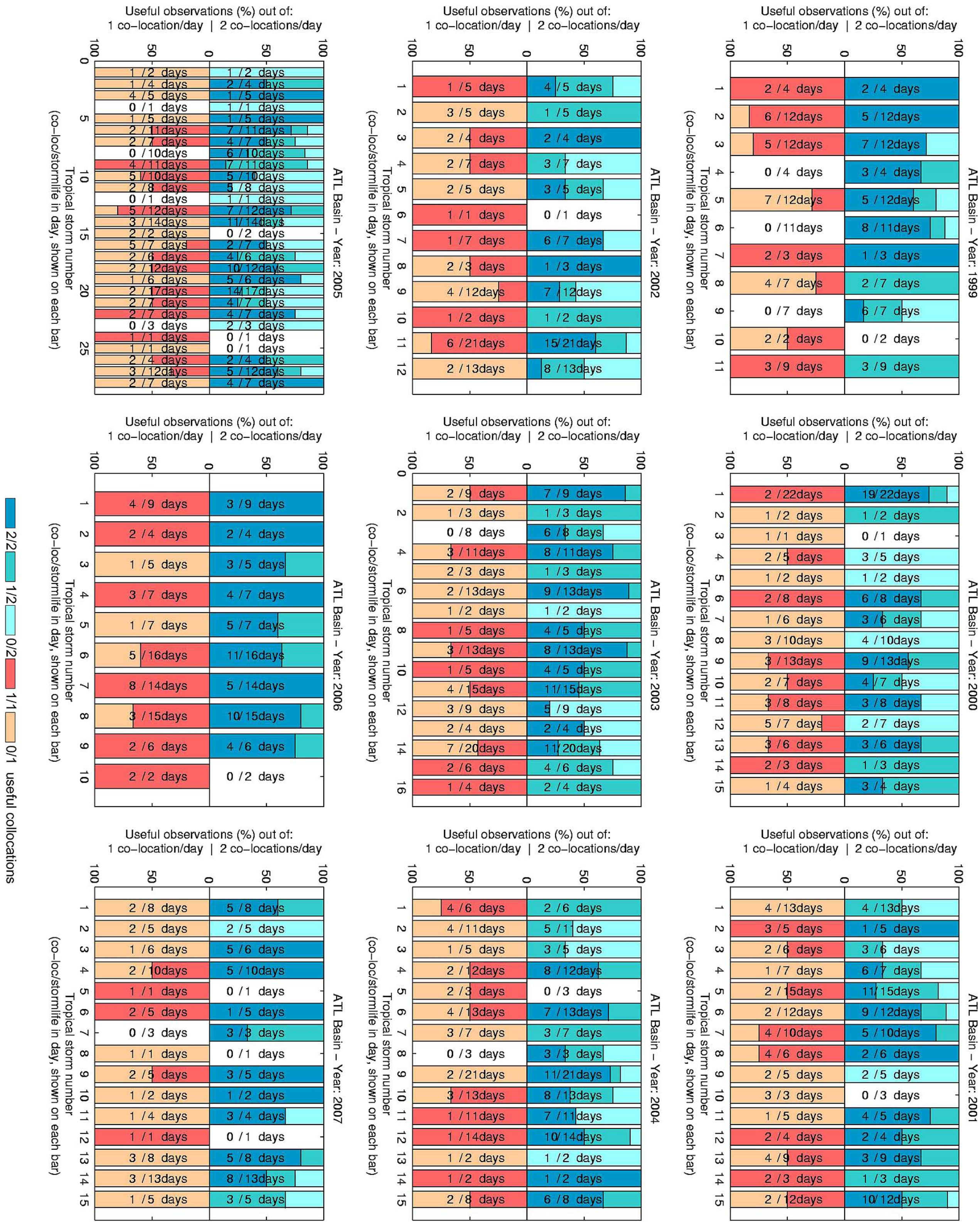

Fig. 9. Bar graphs showing the amount of useful QuikSCAT observations received per TC daily for the ATL basin from 1999 to 2007. On each bar graph, two sets of data are shown: upper bars show statistics for two co-located images obtained daily; lower bars show statistics when only one co-located image is obtained daily. The former scenario has three cases where possibly both obtained images are useful to the analyst, only one is, or none of them are. In the latter scenario, the received image is either useful to the analyst or not. Each of these possibilities is represented in percent on the bar graph for each TC.

different platforms would increase these low results. In any case, judging the usefulness of an image is a subjective task and relies heavily on the analyst's experience in interpreting a QuikSCAT wind field UHR image. Therefore, it may be possible to obtain

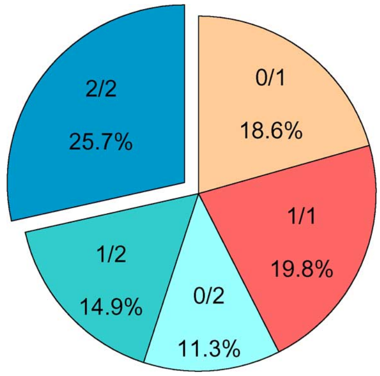

Fig. 10. Pie chart displaying how often useful UHR images are retrieved for TCs of all QuikSCAT images available daily, as noted on each slice (years 1999–2007 combined for the ATL basin). Up to two images can be retrieved per day although in many cases only a single image per day is available. The exploded slices show that two useful (for TC center identification) out of two available images per day were obtained for 25.7% (ATL) of the time between 1999 and 2007.

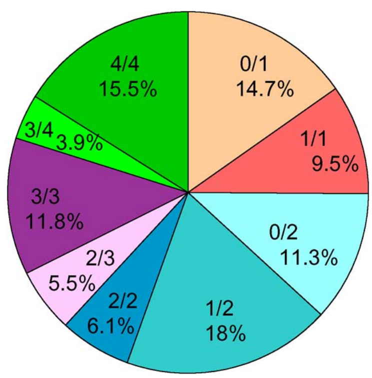

Fig. 11. Pie chart displaying how many useful UHR images are retrieved per day for the ATL basin during the year 2003. During this year, two scatterometers (SeaWinds on ADEOS II and on QuikSCAT) provided UHR images simultaneously which increased temporal coverage. It is then possible to obtain up to four useful UHR images per TC per day.

more useful images per day depending on the analyst's experience in interpreting wind field patterns.

A. Results Obtained From SeaWinds on QuikSCAT and ADEOS II for the Year 2003

For nine months in 2003, two SeaWinds scatterometers were operational (QuikSCAT and ADEOS II). Both devices provided the same wind products at the same daily rate. The orbit phasing ensured that each instrument observes the same location at a different local-time of day. As a result, the amount of useful daily UHR images for TC analysis ideally is doubled. Fig. 11 shows the results obtained for that year. As expected, a maximum of four useful UHR images are available daily (in seldom cases up to five). However, only 15.5% of the time in the Atlantic basin were four out of four daily UHR images useful to the analyst. The chart shows that for about 45% of the time, two or more useful UHR images are available daily, versus 25% when only one scatterometer is available (see pie chart in Fig. 10). As one might expect, two scatterometers measuring wind fields over the ocean and operating simultaneously around the globe provide more critical data on a daily basis for TC analysts.

VI. Conclusion

This paper provides an analysis of QuikSCAT UHR wind product's effectiveness in estimating specific TC parameters such as center location and wind radii. In Section III, QuikSCAT TC UHR passes are visually analyzed and separated into two categories (low and high confidence) depending on the confidence level of identifying the TC center location. This analysis is done based only on scatterometer wind speed and direction fields. TC center identification using high-confidence cases provides similar results compared to best track data. A high-confidence UHR image is therefore useful in obtaining a good estimate of a TC center location. It can be argued that QuikSCAT data is not necessary to identify center location when TCs are well-defined since the center can be identified using infrared or optical satellite imagery. However, a Central Dense Overcast (CDO) can be present, which makes it difficult to find the center using traditional methods. In such cases, QuikSCAT data can be essential. Identifying TC center in a low-confidence case (an underdeveloped TC or a TC with a poorly defined eye) can be difficult, though QuikSCAT wind products are considered useful in identifying developing tropical depressions [28]. Although poor results in determining TC center location are frequent in low-confidence QuikSCAT images, these images are still valuable to the weather community.

Section IV describes and analyzes two ways of estimating wind radii using QuikSCAT UHR data. The first method consists of direct wind radius estimation from QuikSCAT maximum wind speed at a given radius. This estimation is compared with both H*wind and EBT co-located TC cases. The second method proposes the use of a static model and a transfer function applied to QuikSCAT UHR wind product to automatically estimate wind radii for any TC. Validation of the results of this method is performed with co-located EBT cases. Due to the simplicity of this model and the existence of more complex algorithms, this method represents an upper bound on the achievable accuracy. Nevertheless, the results demonstrate that the QuikSCAT UHR wind product can be used to estimate wind radii. The simple automated method assumes knowledge of the center location and intensity category to use the appropriate static model. In a near-real-time application, the center location would have to be identified manually beforehand. Once the latter is estimated, a hurricane forecaster can infer a wind radius estimate from QuikSCAT UHR wind product and adjust it if necessary. Our results suggest that it may only be possible to obtain a wind radius estimate from QuikSCAT a maximum of twice a day due to the nature of QuikSCAT daily ocean coverage. Even with the limited daily coverage QuikSCAT can provide for a given TC, its UHR wind product may be the most reliable source for estimating a TC wind speed field when TCs are out of reach from aircraft.

VII. Postscript

This paper was prepared and submitted prior to the demise of the QuikSCAT primary wind mission, which ended in November 2009 when the spin bearing reached end of life. Though originally designed for only a three-year mission life, the extended QuikSCAT mission demonstrated the value of scatterometry in the study of TCs and proved to be a valuable resource for real-time hurricane tracking [1]. It will be missed. Though no U.S. follow-on mission is currently planned, the Indian Space Research and Development Organization has launched a similar scatterometer on its Oceansat-2 satellite. In addition, the European Space Agency continues to operate a series of C-band fan-beam scatterometers which provide real-time information for weather forecasting.

REFERENCES

[1] J. M. Von Ahn, J. M. Sienkiewicz, and P. S. Chang, "Operational impact of QuikSCAT winds at the NOAA ocean prediction center," *Weather and Forecasting*, vol. 21, no. 4, pp. 523–539, 2006.

[2] R. T. Edson and J. D. Hawkins, "A comparison of scatterometer-derived wind data over tropical cyclones as determined from ERS-2 and QuikSCAT data," in *Proc. AMS 24th Conf. Hurricanes and Tropical Meteorology*, Ft. Lauderdale, FL, 2000.

[3] M. W. Spencer, C. Wu, and D. G. Long, "Improved resolution backscatter measurements with the SeaWinds pencil-beam scatterometer," *IEEE Trans. Geosci. Remote Sens.*, vol. 38, no. 1, pp. 89–104, 2000.

[4] R. N. Hoffman and S. M. Leidner, "An introduction to the near-real-time QuikSCAT data," *Weather and Forecasting*, vol. 20, no. 4, pp. 476–493, Aug. 2005.

[5] S. H. Yueh, B. Stiles, W.-Y. Tsai, H. Hu, and W. T. Liu, "QuikSCAT geophysical model function for hurricane wind and rain," in *Geosci. Remote Sens. Symp.*, Jul. 2001, vol. 3, pp. 1089–1091.

[6] D. W. Draper and D. G. Long, "Evaluating the effect of rain on SeaWinds scatterometer measurements," *J. Geophys. Res.*, vol. 109, no. C02005, 2004.

[7] D. W. Draper and D. G. Long, "Simultaneous wind and rain retrieval using SeaWinds data," *IEEE Trans. Geosci. Remote Sens.*, vol. 42, no. 7, pp. 1411–1423, 2004.

[8] J. R. Allen and D. G. Long, "An analysis of SeaWinds-based rain retrieval in severe weather events," *IEEE Trans. Geosci. Remote Sens.*, vol. 43, no. 12, pp. 2870–2878, 2005.

[9] B. W. Stiles and S. Yueh, "Impact of rain on spaceborne Ku-band scatterometer data," *IEEE Trans. Geosci. Remote Sens.*, vol. 40, pp. 1973–1983, 2002.

[10] T. Lungu, *QuikSCAT Science Data Product User's Manual: Overview and Geophysical Data Products, Version 3.0.* Jet Propulsion Lab., Pasadena, CA, Jun. 2006 [Online]. Available: ftp://podaac.jpl.nasa.gov/pub/ocean_wind/quikscat/doc/QSUG_v3.pdf

[11] R. N. Hoffman and R. S. Dunbar, *SeaWinds Scatterometer Real-Time Merged Geophysical Data Product.* Jet Propulsion Lab., Pasadena, CA, Feb. 2000 [Online]. Available: ftp://podaac.jpl.nasa.gov/near_real_time/ocean_wind/quikscat/doc/nrt_mgdr_guide.pdf

[12] D. Long, J. Luke, and W. Plant, "Ultra high resolution wind retrieval for SeaWinds," in *Proc. Int. Geoscience and Remote Sensing Symp.*, Toulouse, France, Jul. 2003, pp. 1264–1266.

[13] M. P. Owen and D. G. Long, "Simultaneous wind and rain estimation for QuikSCAT at ultra-high resolution," *IEEE Trans. Geosci. Remote Sens.*, 2011, doi: 10.1109/TGRS.2010.2102361.

[14] B. A. Williams and D. G. Long, "A reconstruction approach to scatterometer wind vector field retrieval," *IEEE Trans. Geosci. Remote Sens.*, vol. 49, no. 7, Jul. 2011, doi: 10.1109/TGRS.2010.2100402 .

[15] B. A. Williams and D. G. Long, "Reconstruction from aperture-filtered samples with application to scatterometer image reconstruction," *IEEE Trans. Geosci. Remote Sens.*, vol. 49, no. 5, pp. 1663–1676, May 2011.

[16] B. A. Williams and D. G. Long, "Estimation of hurricane winds from SeaWinds at ultrahigh resolution," *IEEE Trans. Geosci. Remote Sens.*, vol. 46, no. 10, pp. 2924–2935, Oct. 2008.

[17] B. A. Williams, M. P. Owen, and D. G. Long, "The ultra high resolution QuikSCAT product," in *Proc. 2009 IEEE Radar Conf.*, Pasadena, CA, 2009.

[18] J. L. Demuth, M. DeMaria, and J. A. Knaff, "Improvement of advanced microwave sounding unit tropical cyclone intensity and size estimation algorithms," *J. Appl. Meteorol. Climatol.*, vol. 45, no. 11, pp. 1573–1581, 2006.

[19] F. Saïd, "An evaluation of QuikSCAT UHR wind product's effectiveness in determining selected tropical cyclone characteristics," Master thesis, Brigham Young Univ., Provo, UT, 2009.

[20] R. T. Edson, M. A. Lander, C. E. Cantrell, J. L. Franklin, P. S. Chang, and J. D. Hawkins, "Operational use of quikscat over tropical cyclones," presented at the AMS 25th Conf. Hurricanes and Tropical Meteorology, San Diego, CA, 2002.

[21] C. Weatherford and W. M. Gray, "Typhoon structure as revealed by aircraft reconnaissance. Part II: Structural variability," *Monthly Weather Review*, vol. 116, pp. 1044–1056, 1988.

[22] Hurricane Hunters Assoc., The Mission of the Hurricane Hunters [Online]. Available: http://www.hurricanehunters.com/mission.html

[23] M. D. Powell, S. H. Houston, L. R. Amat, and N. Morisseau-Leroy, "The HRD real-time hurricane wind analysis system," *J. Wind Eng. Indust. Aerodyn.*, vol. 77&78, 1998.

[24] Central Florida Remote Sensing Lab, Department of Atmospheric Sciences, UNC Asheville, NASA Ocean Vector Winds [Online]. Available: http://cyclone.atms.unca.edu/quikscat/hwind.html 2008

[25] S. C. for Applications and Research, Mark Demaria Cooperative Research Program [Online]. Available: http://www.star.nesdis.noaa.gov/star/DeMaria_M.php

[26] D. R. Chavas and K. A. Emanuel, "A QuikSCAT climatology of tropical cyclone size," *Geophys. Res. Lett.*, vol. 37, no. L188116, 2010, doi: 10.1029/2010GL044558.

[27] Remote Sensing Systems, Description of Scatterometer Data Products Feb. 2009 [Online]. Available: http://www.ssmi.com/qscat/qscat_description.html

[28] K. B. Katsaros, E. B. Forde, P. Chang, and W. T. Liu, "QuikSCAT's SeaWinds facilitates early identification of tropical depressions in 1999 hurricane season," *Geophys. Res. Lett.*, vol. 28, no. 6, pp. 1043–1046, Mar. 2001.

Faozi Saïd received the M.S. degree in electrical engineering from Brigham Young University (BYU), Provo, UT, in 2009. He is currently working toward the Ph.D. degree in physics at the University of Tromsø, Norway.

His current research interests include microwave remote sensing, SAR signal processing, and sea surface dynamics.

David G. Long (S'80–SM'98–F'08) received the Ph.D. degree in electrical engineering from the University of Southern California, Los Angeles, in 1989.

From 1983 to 1990, he worked for NASA's Jet Propulsion Laboratory (JPL) where he developed advanced radar remote sensing systems. While at JPL he was the Project Engineer on the NASA Scatterometer (NSCAT) project which flew from 1996 to 1997. He also managed the SCANSCAT project, the precursor to SeaWinds which was launched in 1999 and 2002. He is currently a Professor of the Electrical and Computer Engineering Department at Brigham Young University where he teaches upper division and graduate courses in communications, microwave remote sensing, radar, and signal processing and is the director of the BYU Center for Remote Sensing. He is the principle investigator on several NASA-sponsored research projects in remote sensing. He has over 400 publications in signal processing and radar scatterometry. His research interests include microwave remote sensing, radar theory, space-based sensing, estimation theory, signal processing, and mesoscale atmospheric dynamics.

Dr. Long has received the NASA Certificate of Recognition several times. He is currently an Associate Editor for IEEE *Geoscience and Remote Sensing Letters*.